

Article

Highly-Efficient Longitudinal Second-Harmonic Generation from Doubly-Resonant AlGaAs Nanoantennas

Lei Xu ¹, Mohsen Rahmani ², Daria Smirnova ^{2,3} , Khosro Zangeneh Kamali ², Guoquan Zhang ⁴ , Dragomir Neshev ²  and Andrey E. Miroshnichenko ^{1,*}

¹ School of Engineering and Information Technology, University of New South Wales, Canberra ACT 2600, Australia; lei.xu@unsw.edu.au

² Nonlinear Physics Centre, Research School of Physics and Engineering, The Australian National University, Canberra ACT 0200, Australia; Mohsen.Rahmani@anu.edu.au (M.R.); fade.margin@gmail.com (D.S.); khosro.zangeneh@gmail.com (K.Z.K.); dragomir.neshev@anu.edu.au (D.N.)

³ Institute of Applied Physics, Russian Academy of Sciences, 603950 Nizhny Novgorod, Russia

⁴ The MOE Key Laboratory of Weak-Light Nonlinear Photonics, School of Physics and TEDA Applied Physics Institute, Nankai University, Tianjin 300457, China; zhanggq@nankai.edu.cn

* Correspondence: andrey.miroshnichenko@unsw.edu.au

Received: 23 August 2018; Accepted: 13 September 2018; Published: 17 September 2018



Abstract: We design an asymmetric nonlinear optical nanoantenna composed of a dielectric nanodisc and an adjacent nanobar. The proposed composite structure made of AlGaAs exhibits resonant response at both the fundamental and doubled frequencies. Being driven by the strong magnetic dipole resonance at the pump wavelength and a high-quality mode at the harmonic wavelength, the efficient second-harmonic radiation is generated predominantly along the vertical directions under the normally incident plane-wave excitation.

Keywords: scattering; second-harmonic generation; Mie resonance; nanoantenna; multipolar interference

1. Introduction

Nonlinear nanophotonics is a rapidly developing research field with various applications including nonlinear light sources [1], ultrafast chip-based optoelectronic devices [2], nonlinear microscopy and spectroscopy techniques [3] and bioimaging and sensing [4]. Exploiting nonlinear optical effects in nanostructures plays an important role in the implementation of miniature nonlinear photonic components for further integration of multiple optical functionalities into a single compact optical chip. To this purpose, nonlinear nanoplasmonics has been widely studied both theoretically and experimentally during the last decade [5–10]. However, its performance is restricted by the high ohmic losses, small mode volumes and low laser damage threshold. High-index all-dielectric nanostructures provide a powerful platform for controlling light at the nanoscale [11,12]. They offer unique opportunities to boost the nonlinear effects due to the strong near-field enhancement associated with the excitation of Mie-type resonances [13,14]. In recent years, various fabrication techniques, including lithography, chemical methods, dewetting, etc., have been developed for the realization of all-dielectric nanostructures, greatly paving the way for low-cost manufacturing of all-dielectric nanostructures [15–17]. Via engineering and control over the optically-induced electric and magnetic resonances in all-dielectric nanostructures, both high nonlinear conversion efficiency and directivity of the harmonic radiation pattern can be achieved. Nanostructures made of high-index semiconductors with a strong nonlinear response, such as Si, Ge, which possess a large third-order susceptibility,

have been investigated widely for third-harmonic generation, showing huge nonlinear enhancement when exciting the nanostructure in the vicinity of Mie resonances, particularly magnetic dipole (MD) resonance [18], Fano resonance or collective modes [19–21] and anapole states [22–25]. In contrast to the third-order nonlinearity, Si and Ge do not possess bulk second-order nonlinearity due to their centrosymmetric crystalline structure [26]. However, III-V semiconductors, such as GaAs or AlGaAs, show a strong second-order nonlinear response due to their large bulk second-order optical susceptibility $\chi^{(2)}$, representing a great deal of interest because of their strong nonlinear effects and optoelectronic properties [27]. By engineering the AlGaAs alloy composition, two-photon absorption can be avoided at the telecommunication wavelengths, enabling high transparency in a broad spectral window from visible to far infrared. Both theoretical and experimental studies have been performed to enhance the second-harmonic generation (SHG) process in GaAs or AlGaAs Mie resonators [28–34]. The SHG from AlGaAs nanoantennas has been predicted to reach conversion efficiency of 10^{-3} , and later, efficiency of 10^{-4} was measured experimentally by exploiting the magnetic dipole (MD) resonance [28,31]. However, when employing AlGaAs structures, despite the high conversion efficiency, there were no emitted second-harmonic (SH) signal observed in both the forward and backward normal directions. The absence of the emission at normal directions is due to the specific nonlinear susceptibility tensor of [100]-grown zinc-blend AlGaAs crystalline structures, which only contain off-diagonal elements $\chi_{ijk}^{(2)}$ with $i \neq j \neq k$. It limits the collected nonlinear signal and restricts many photonic applications, e.g., highly-efficient nonlinear light sources and nonlinear spectroscopy.

In this work, we present a theoretical study on the resonant multipolar effects in AlGaAs nanoantennas in both linear and nonlinear responses. Then, we propose and design an asymmetric AlGaAs nanoantenna composed of a nanodisc and an adjacent nanobar. Under normally incident pump, our nanoantenna supports resonant responses at both the fundamental and harmonic wavelengths, enabling a high second-harmonic conversion efficiency of the order of 10^{-3} at the pump intensity of $I_0 = 1 \text{ GW/cm}^2$ and also normal SH emission due to the specifically distributed induced nonlinear currents and resonant modes supported by both nanodisc and nanobar. Such highly-efficient longitudinal SH emission has not been realized in [100]-grown AlGaAs nanoantennas to date. Our results may offer new opportunities for the design of new types of novel nonlinear photonic metadevices.

2. Results and Discussion

2.1. Theoretical Model and Numerical Simulations

In our theoretical model, we fixed the thickness of our nanostructures to be $h_0 = 400 \text{ nm}$. The pump is y-polarized with a wavelength of 1550 nm. The widely-used [100]-grown AlGaAs material is considered as the platform for our nanostructures. The second-order nonlinear susceptibility tensor of [100]-grown AlGaAs, possessing a zinc blend crystalline structure, is anisotropic and has only off-diagonal elements $\chi_{ijk}^{(2)}$ with $i \neq j \neq k$. Thus, in the principal-axis system of the crystal, the i -th component of the nonlinear polarization at the SH frequency is given by:

$$P_i^{2\omega} = \epsilon_0 \chi_{ijk}^{(2)} E_j^\omega E_k^\omega. \quad (1)$$

We use the FEM solver in COMSOL Multiphysics (Version 5.3) in the frequency domain to model both the linear and nonlinear responses of such nanoantennas. First, we simulate the linear scattering at the fundamental frequency. The bulk nonlinear polarization induced inside the particle is then employed as a source for the electromagnetic simulation to obtain the generated SH field. The value of $\chi_{ijk}^{(2)}$ in the simulation is 100 pm/V [28]. The material dispersion of AlGaAs is deduced from [35,36].

2.2. Linear and Nonlinear Responses from a Single AlGaAs Nanodisc

The electric and magnetic Mie resonances in all-dielectric nanostructures allow for flexibly engineering the multipolar excitation and control of the optical responses for enhancing the near-field interactions and far-field radiation shaping. Through a geometric tuning, the nanoantenna can support resonant effects at several wavelengths simultaneously. We first optimize our nanoantennas to support strong resonant responses at both 1550 nm and 775 nm, corresponding to the pump and harmonic wavelengths in our case. Figure 1 shows the linear scattering characteristics, the total linear scattering efficiency Q and corresponding multipolar contributions of free-standing AlGaAs nanodiscs with increasing disk radius under normal plane wave excitation [28]. As can be seen in Figure 1, a broad mode (Mode A) dominated by MD resonance associated with partly excited electric dipole (ED) resonance is obtained for a nanodisc of radius $r_0 = 215$ nm at the fundamental wavelength. This mode allows for a strong near-field enhancement with confined electromagnetic energy inside the nanodisc, as shown in Figure 2a–c. At the SH wavelength, the scattering spectrum shows a sharp peak corresponding to a resonant mode (Mode B) near $r_0 = 215$ nm. This mode is formed by the excitation of and interference between ED, MD, electric quadrupole (EQ) and electric octupole (EO) resonances. By calculating the complex frequency of the eigenmodes using the FEM solver through eigenfrequency analysis in COMSOL Multiphysics, the Qfactor of Mode B is estimated to be 52. These high-quality modes supported by the nanoantenna result in an enhanced near-field distributions, as shown in Figure 2e–g. Further investigation of the far-field pattern shows that both radiation patterns at these two wavelengths are characterized by a main lobe in the forward directions, featuring the Kerker's condition due to the interference between the excited ED and MD resonances. While the slightly narrower lobe for the pattern at SH wavelength is due to the suppression of the side-lobe scattering based on the interference between the same type of excited multipoles of different orders (ED, EQ, EO).

Optically pumping the nanoantenna in the vicinity of Mode A and simultaneously exciting the resonant multipolar response driven by Mode B during the nonlinear process allow achieving spectral and spatial mode overlap at both fundamental and SH wavelengths. In this case, the SH conversion efficiency is expected to be boosted, as well as achieving longitudinal SH emission based on the multipolar interference effect. It is worth mentioning that the nanodisc supports other modes around the SH wavelength of 775 nm besides Mode B. These modes are not excited under normal plane wave incidence, while they can be excited under proper pump irradiation conditions, for example using special vector beam irradiation, which has large spatial overlap between the electric fields of the pump beam and the resonator mode [37,38]. In the following, we will focus on exploring the SHG process in the vicinity of the above-mentioned Mode A (near the pump wavelength) and Mode B (near the harmonic wavelength) to achieve doubly-resonant normal SH emission in AlGaAs nanoantennas.

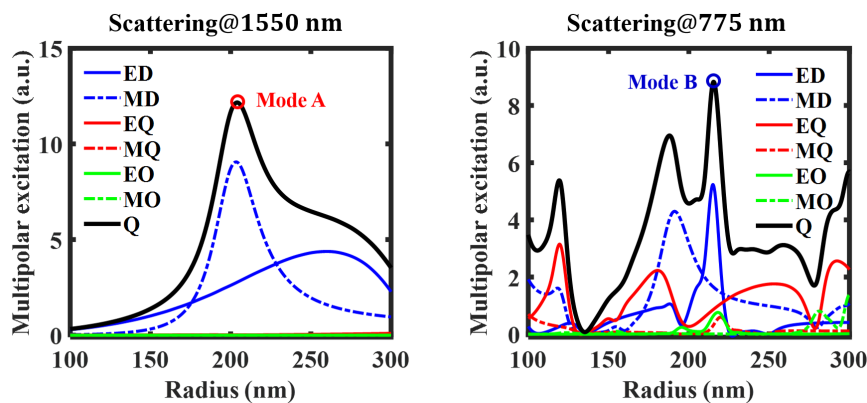


Figure 1. Multipolar decomposition of linear light scattering by AlGaAs nanodiscs with different radii for normal plane wave incidence at the wavelengths of (a) $\lambda = 1550$ nm and (b) $\lambda = 775$ nm, respectively. ED, electric dipole; MD, magnetic dipole; EQ, electric quadrupole; MQ, magnetic quadrupole; EO, electric octupole; MO, magnetic quadrupole.

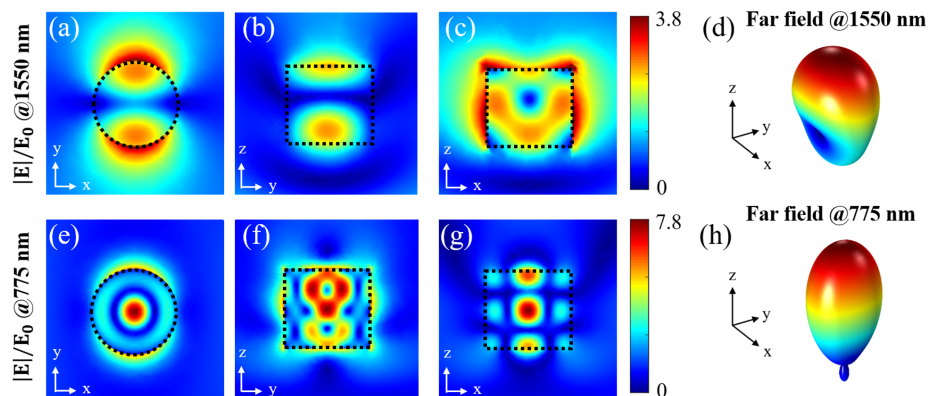


Figure 2. Near-field distributions of the electric field magnitude for the nanodisc radius being $r_0 = 215$ nm at the pump wavelength of (a–c) $\lambda = 1550$ nm and (e–g) $\lambda = 775$ nm, and the corresponding far-field patterns at the pump wavelength of (d) $\lambda = 1550$ nm and (h) $\lambda = 775$ nm, respectively.

The generated nonlinear multipoles inside the nanoantenna are driven by the induced nonlinear currents. Thus, by controlling the induced nonlinear currents, we can further obtain the excitation of a specific mode, i.e., a combination of and interferences between several specific nonlinearly-generated multipoles, to enable desirable directivity of the radiation pattern, as well as resonantly-enhanced conversion efficiency.

To enable strong resonant response at 775 nm driven by Mode A during the nonlinear process, one possible method is to generate nonlinear polarization within the transverse plane, imitating the mode polarization distribution, which is similar to the case when using normal plane wave irradiation. The second-order nonlinear susceptibility tensor of the [100]-grown AlGaAs possesses a zinc-blend crystalline structure containing only off-diagonal elements $\chi_{ijk}^{(2)}$ with $i \neq j \neq k$. Thus, in order to induce the nonlinear polarization within the transverse plane, the excited MD resonance needs to be rotated to along $\pi/4$ to the transverse plane. For our designed AlGaAs nanodisc with a similar size in each direction, this can be simply achieved by tilting the incident pump. For example, optically pumping along $\pi/4$ will excite an MD oriented along $\pi/4$, resulting in induced nonlinear polarization vectors mainly within the transverse plane. Based on Figure 1b, this induced nonlinear polarization is expected to possess strong resonant response at 775 nm driven by Mode A. The calculated near-field distributions at fundamental and harmonic wavelengths are shown in

Figure 3a,b, respectively. It is clearly shown that the SH near-field distribution resembles Mode B in Figure 2, revealing the resonant response of SH emission driven by Mode B. Figure 3c shows the SH far-field pattern. The SH conversion efficiency is estimated to be of the order of 10^{-3} using a pump intensity of $I_0 = 1 \text{ GW/cm}^2$, demonstrating both high efficiency and normal emission in this case. This feature has been previously mentioned in [32].

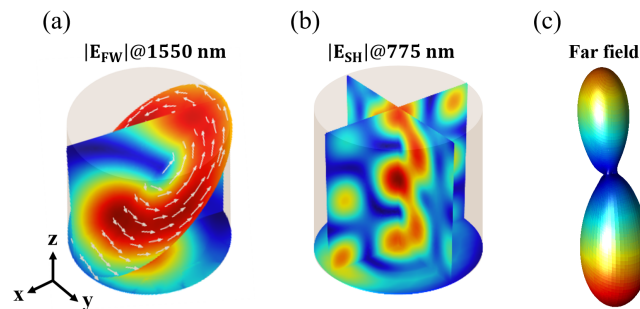


Figure 3. Near-field distributions of electric field magnitude at the fundamental wavelength (a) and harmonic wavelength (b), respectively. (c) gives the second-harmonic radiation pattern.

This can also be interpreted from the overlap between the nonlinear currents and the specified mode, which is defined as:

$$\zeta = \frac{|\int \mathbf{E}_r^* \cdot \mathbf{J}_i dV|^2}{\int |\mathbf{E}_r|^2 dV \int |\mathbf{J}_i|^2 dV} \quad (2)$$

where \mathbf{E}_r is the resonant mode at the harmonic wavelength and \mathbf{J}_i is the induced nonlinear current by a given pump.

As shown in Figure 4, the maximum SH conversion efficiency happens when the overlap reaches its maximum. The multipolar excitation varies with increasing pump tilt angle θ , resulting in reshaping of the SH far-field pattern (see Figures 3c and 4c,d). A strong normal SH emission takes place under pump beam tilt angle $\theta = \pi/4$, where the overlap between the nonlinear currents and Mode B is around 0.3 (Figure 2c). Compared with the multipolar excitation shown in Figure 1b and far-field pattern shown in Figure 2h, the lack of excitation of sizeable MD and EQ further weakens the Kerker’s condition and leads to an SH emission pattern in both forward and backward directions (as shown in Figure 3c).

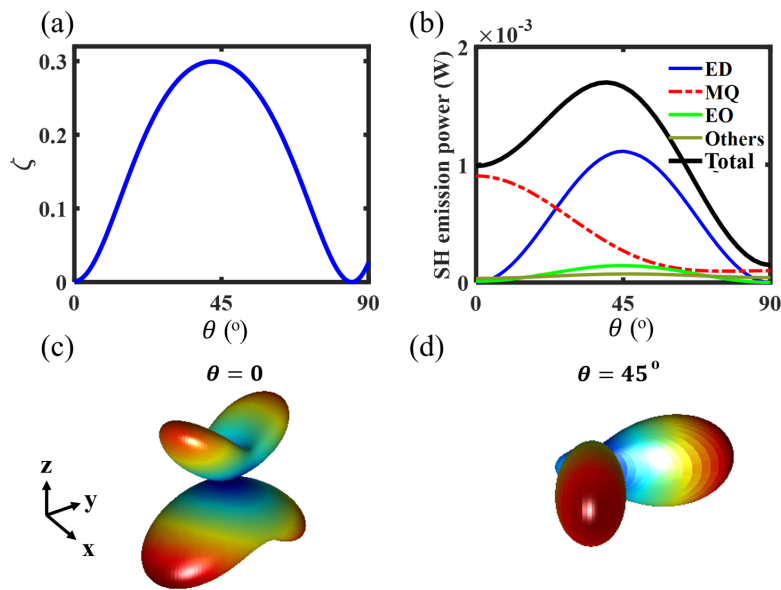


Figure 4. (a) Calculated overlap ζ for different pump tilt angle; (b) the multipolar structure of SH emission with different pump tilt angle. (c,d) gives the far-field patterns for pump tilt angle $\theta = 0^\circ$ and 45° , respectively.

The unique tensorial susceptibility of AlGaAs material enables the polarization dependent nonlinear emission on the pump [31,33]. By simply varying the angle θ_c between the crystalline axis and laboratory coordinate x (or y) axis within the transverse plane, the nonlinearly generated electric and magnetic multipoles can be tuned slightly. The SH conversion efficiency increases with increasing θ_c from 0° – 45° . This polarization dependence of SHG also provides a simple method to determine the crystalline orientation of AlGaAs nanoantennas [39]. Importantly, the SH emission maintains high directivity, i.e., normal emission under different rotating angle θ_c , as shown in Figure 5.

However, considering practicability, where objectives are used to both excite the nanoantenna and collect the signals [31], after tilting the incident pump experimentally, the collection of the normal harmonic emission remains a problem. Approaches to obtain normal harmonic emission by normal pump incidence are yet to be developed.

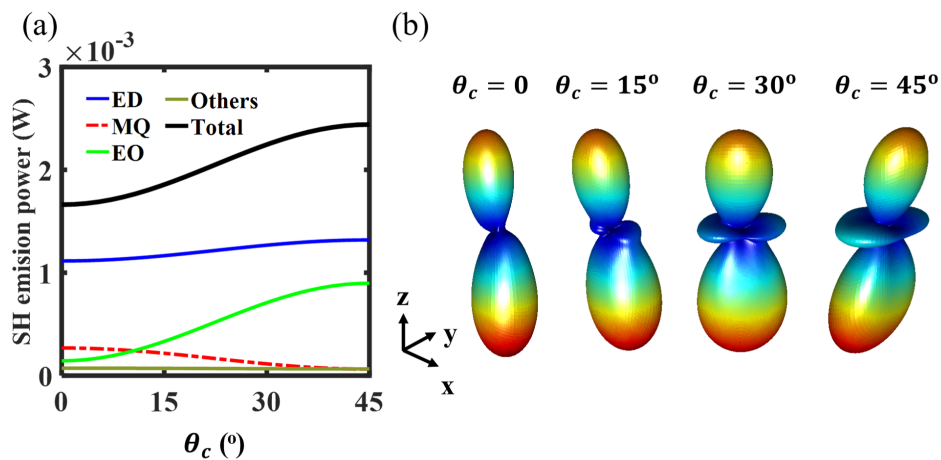


Figure 5. Nonlinear emission under oblique pump incidence with $\theta = 45^\circ$. (a) Nonlinear multipolar excitation for different rotating angle θ_c ; (b) the far-field patterns for different rotating angle θ_c .

2.3. Longitudinal SHG through a Doubly-Resonant AlGaAs Nanoantenna

As discussed above, by exciting 45° -oriented MD resonance at the fundamental wavelength, it is possible to induce a parallel-oriented nonlinear polarization from AlGaAs nanoantenna and furthermore obtain the resonant response of SH emission driven by Mode B at the harmonic wavelength. Unfortunately, for a nanodisc under normal pump incidence, the excitation of 45° -oriented MD resonance is not possible due to the symmetry protection. However, by breaking the symmetry of our nanoantenna, it is possible to control the orientation of excited MD resonance. Here, we further introduce an adjacent elongated nanobar to support a broad ED resonance to control the MD excitation of the nanodisc [40]. The schematic of the designed nanoantenna is shown in Figure 6a. It is worth noting that the material and size of the nanobar are also flexible and not restricted to AlGaAs in this approach. Here, for practical purposes, the thickness and material are set to be the same as the nanodisc. As an example, the gap between the disk and the nanobar is set to be $g = 100$ nm, and the size of the nanobar is set to be length $L = 200$ nm and width $w = 900$ nm, to support a strong coupling between the resonances supported by the nanobar and nanodisc. Under normal pump incidence, the MD supported by the nanodisc can be engineered through the interaction with the ED resonance supported by the nanobar. As a result, the MD resonances is re-oriented along 45° to the in-plane direction, similar to the case of oblique pump excitation on a single nanodisc (see Figure 3a). Thus, in the vicinity of Mode B supported by the nanodisc, this MD resonance will further excite strong multipolar resonances during the nonlinear process, leading to highly-efficient normal nonlinear emission.

Figure 6b shows the near-field distributions at the fundamental wavelength; the 45° -oriented circular field distribution reveals the excitation of MD resonance along 45° to the in-plane direction. We further use the internal field inside the nanoantenna to perform the multipolar decomposition for the nanodisc and nanobar separately, as shown in Figure 6c,d. For the disk radius $r_0 = 215$ nm, an ED resonance is excited within the nanobar, while an MD resonance is excited within the nanodisc with the suppression of ED resonance, exhibiting also anapole state excitation for the disk radius $r_0 = 215$ nm. This will further benefit our target to achieve highly-efficient normal emission driven by Mode B supported by the nanodisc: for a nonlinear process, MD resonance has been well known for its ability to boost the nonlinear process due to the near-field enhancement inside the nanostructure, while for ED resonance, most of the electric energy is located near the edges of the nanostructure, and its ability to enhance the nonlinear process is restricted.

We first investigate the SH emission enhancement through such doubly-resonant nanoantennas. Figure 7a gives the calculated SH emission power as a function of the disk radius. By optically pumping near MD resonance, we are able to obtain strong SH enhancement at the harmonic wavelength in the vicinity of Mode A position $r_0 = 215$ nm. Meanwhile, an emission peak also occurs around a disk radius of 202.5 nm. This peak is driven by another mode supported by the nanoantenna at this position, resulting from the alignment of the induced nonlinear current and the mode. However, the far-field pattern from this strong SH emission is nearly null in the forward and backward directions, as shown in the inset of Figure 7a, different from the SH emission pattern driven by Mode B (shown in the following Figure 8).

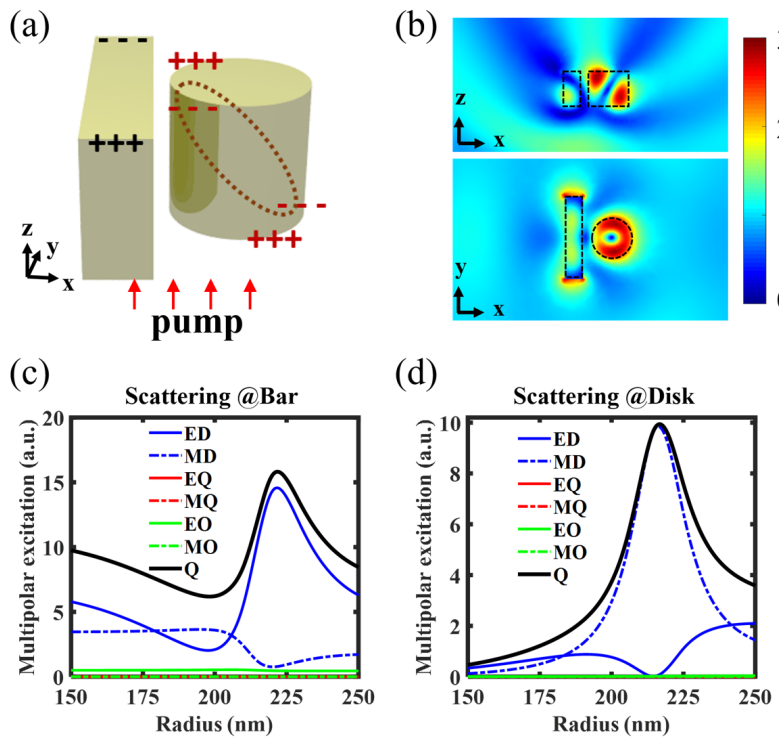


Figure 6. (a) Schematic of the designed asymmetric AlGaAs nanoantennas; (b) near-field distribution of the electric field under the normal plane wave pump with wavelength $\lambda = 1550$ nm; (c) multipolar excitations within the nanobar as a function of the disk radius; (d) multipolar excitation within the nanodisk as a function of the disk radius.

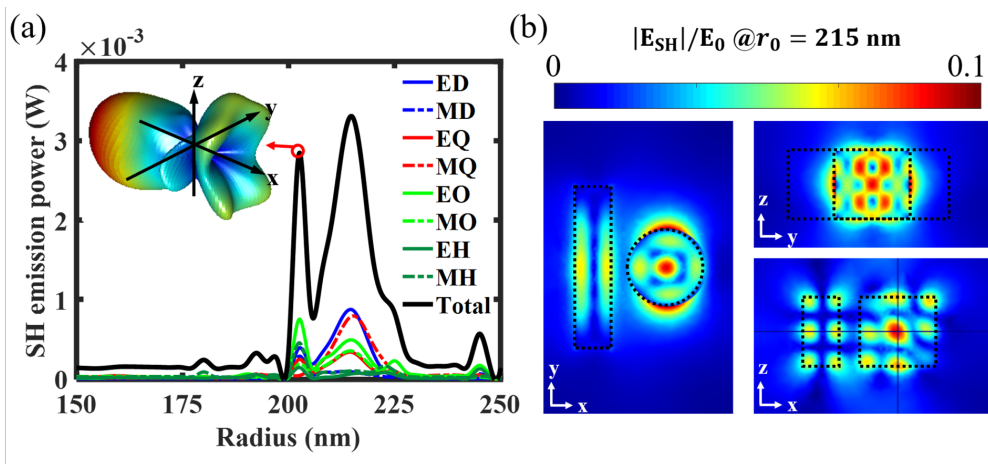


Figure 7. (a) Calculated SH emission power and the nonlinear multipolar structure with different disk radii. The inset shows the corresponding SH far-field pattern for disk radius $r_0 = 202.5$ nm. (b) Near-field distributions of the SH electric field magnitude for disk radius $r_0 = 215$ nm. $\theta_c = 0$.

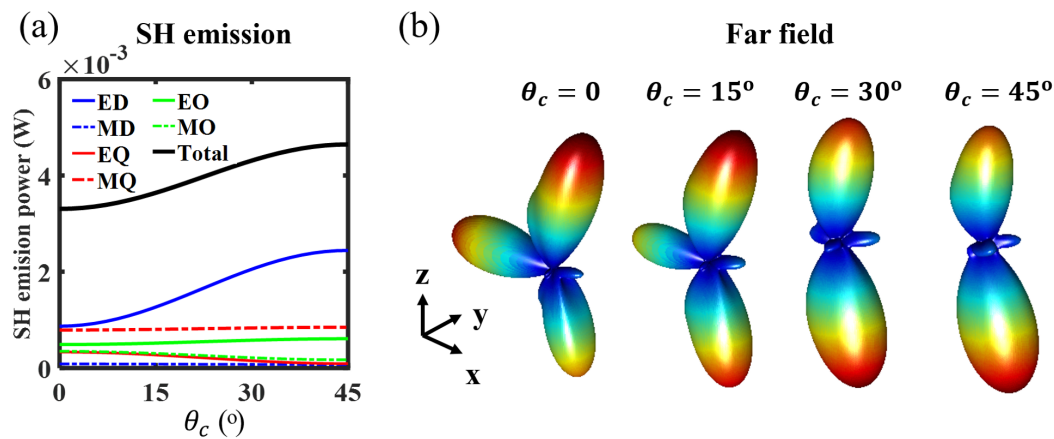


Figure 8. (a) Calculated SH emission power and the nonlinear multipolar structure as a function of θ_c ; (b) the far-field patterns for different rotating angles θ_c .

Figure 7b shows the near-field distributions corresponding to the SH emission peak at disk radius $r_0 = 215$ nm. It resembles the field of Mode B in Figure 2e–g, revealing the resonant response driven by Mode B at the harmonic wavelength. By further tuning the crystalline angle θ_c , we are able to slightly tune the nonlinearly generated multipoles. Figure 8a shows the nonlinear multipolar excitation as a function of the rotating angle θ_c . Generally, with increasing θ_c from 0° – 45° , the excitation of electric dipole resonance increases with other types of multipoles remaining almost unchanged during the nonlinear process. These multipolar excitations further enable longitudinal SH emissions for different θ_c and a stronger side-lobe suppression in the far-field radiation patterns for larger θ_c (Figure 8b).

3. Conclusions

In summary, we have demonstrated numerically SHG enhancement based on doubly-resonant AlGaAs nanoantennas. By exploiting the modes supported at the harmonic wavelength, it is possible to shape the SH emission pattern and achieve high directivity. Specifically, we have focused on the SHG process driven by the MD resonance at the fundamental wavelength and a high-quality mode at the harmonic wavelength, which leads to normal emission due to the multipolar interference effect. It is shown that by introducing a nanobar adjacent to the nanodisc, it is possible to achieve highly-efficient longitudinal SH emission under normal pump incidence. Our results demonstrate a method to enhance the nonlinear emission and shape the nonlinear radiation pattern through the control of the induced nonlinear currents, which can be useful for applications such as efficient nonlinear light sources and nonlinear spectroscopy.

Author Contributions: Conceptualization, A.E.M., L.X.; Methodology, M.R. and K.Z.K.; Software, L.X. and D.S.; Validation, A.E.M., L.X. and D.N.; Formal Analysis, L.X., M.R., G.Z., D.N. and A.E.M.; Investigation, L.X. and M.R.; Resources, D.S.; Data Curation, L.X., A.E.M. and D.S.; Writing—Original Draft Preparation, L.X. and A.E.M.; Writing—Review & Editing, A.E.M., D.S., M.R., K.Z.K., G.Z. and D.N.; Visualization, L.X. and A.E.M.; Supervision, A.E.M.; Project Administration, A.E.M.; Funding Acquisition, A.E.M., M.R., D.S. and G.Z.

Funding: This research was funded by the Australian Research Council (ARC), ARC Discovery Early Career Research Fellowship (DE170100250) and the Russian Foundation for Basic Research (Grants No. 16-02-00547, 18-02-00381), UNSW Scientia Fellowship and NSFC (No. 11774182, No. 91750204).

Conflicts of Interest: The authors declare no conflict of interest.

References

1. Solntsev, A.; Carletti, L.; Xu, L.; Poddubny, A.; De Angelis, C.; Leo, G.; Kivshar, Y.; Neshev, D.N.; Sukhorukov, A.A. Quantum-classical correspondence for photon-pair generation in nonlinear dielectric nano-resonators. In *Nonlinear Photonics*; Optical Society of America: Washington, DC, USA, 2016; p. NT3A-4.
2. van Sark, W.G.; de Wild, J.; Rath, J.K.; Meijerink, A.; Schropp, R.E. Upconversion in solar cells. *Nanoscale Res. Lett.* **2013**, *8*, 81. [[CrossRef](#)] [[PubMed](#)]
3. Bautista, G.; Kauranen, M. Vector-field nonlinear microscopy of nanostructures. *ACS Photonics* **2016**, *3*, 1351–1370. [[CrossRef](#)]
4. DaCosta, M.V.; Doughan, S.; Han, Y.; Krull, U.J. Lanthanide upconversion nanoparticles and applications in bioassays and bioimaging: A review. *Anal. Chim. Acta* **2014**, *832*, 1–33. [[CrossRef](#)] [[PubMed](#)]
5. Klimov, V. *Nanoplasmonics: Fundamentals and Applications*; Pan Stanford: Singapore, 2012.
6. Lippitz, M.; van Dijk, M.A.; Orrit, M. Third-harmonic generation from single gold nanoparticles. *Nano Lett.* **2005**, *5*, 799–802. [[CrossRef](#)] [[PubMed](#)]
7. Aouani, H.; Rahmani, M.; Navarro-Cía, M.; Maier, S.A. Third-harmonic-upconversion enhancement from a single semiconductor nanoparticle coupled to a plasmonic antenna. *Nat. Nanotechnol.* **2014**, *9*, 290–294. [[CrossRef](#)] [[PubMed](#)]
8. Kim, S.; Jin, J.; Kim, Y.J.; Park, I.Y.; Kim, Y.; Kim, S.W. High-harmonic generation by resonant plasmon field enhancement. *Nature* **2008**, *453*, 757–760. [[CrossRef](#)] [[PubMed](#)]
9. Hanke, T.; Cesar, J.; Knittel, V.; Trügler, A.; Hohenester, U.; Leitenstorfer, A.; Bratschkitsch, R. Tailoring spatiotemporal light confinement in single plasmonic nanoantennas. *Nano Lett.* **2012**, *12*, 992–996. [[CrossRef](#)] [[PubMed](#)]
10. Hentschel, M.; Utikal, T.; Giessen, H.; Lippitz, M. Quantitative modeling of the third harmonic emission spectrum of plasmonic nanoantennas. *Nano Lett.* **2012**, *12*, 3778–3782. [[CrossRef](#)] [[PubMed](#)]
11. Rahmani, M.; Xu, L.; Miroshnichenko, A.E.; Komar, A.; Camacho-Morales, R.; Chen, H.; Zárate, Y.; Kruk, S.; Zhang, G.; Neshev, D.N.; et al. Reversible Thermal Tuning of All-Dielectric Metasurfaces. *Adv. Funct. Mater.* **2017**, *27*, 1700580. [[CrossRef](#)]
12. Nemati, A.; Wang, Q.; Hong, M.; Teng, J. Tunable and reconfigurable metasurfaces and metadevices. *Opto-Electron. Adv.* **2018**, *1*, 18000901–18000925. [[CrossRef](#)]
13. Kuznetsov, A.I.; Miroshnichenko, A.E.; Brongersma, M.L.; Kivshar, Y.S.; Luk'yanchuk, B. Optically resonant dielectric nanostructures. *Science* **2016**, *354*, aag2472. . [[CrossRef](#)] [[PubMed](#)]
14. Smirnova, D.; Kivshar, Y.S. Multipolar nonlinear nanophotonics. *Optica* **2016**, *3*, 1241–1255. [[CrossRef](#)]
15. Liu, S.; Keeler, G.A.; Reno, J.L.; Sinclair, M.B.; Brener, I. III–V semiconductor nanoresonators—A new strategy for passive, active, and nonlinear all-dielectric metamaterials. *Adv. Opt. Mater.* **2016**, *4*, 1457–1462. [[CrossRef](#)]
16. Baranov, D.G.; Zuev, D.A.; Lepeshov, S.I.; Kotov, O.V.; Krasnok, A.E.; Evlyukhin, A.B.; Chichkov, B.N. All-dielectric nanophotonics: The quest for better materials and fabrication techniques. *Optica* **2017**, *4*, 814–825. [[CrossRef](#)]
17. Cao, Y.; Xie, F.; Zhang, P.; Li, X. Dual-beam super-resolution direct laser writing nanofabrication technology. *Opto-Electron. Eng.* **2017**, *44*, 1133–1145.
18. Shcherbakov, M.R.; Neshev, D.N.; Hopkins, B.; Shorokhov, A.S.; Staude, I.; Melik-Gaykazyan, E.V.; Decker, M.; Ezhov, A.A.; Miroshnichenko, A.E.; Brener, I.; et al. Enhanced Third-Harmonic Generation in Silicon Nanoparticles Driven by Magnetic Response. *Nano Lett.* **2014**, *14*, 6488–6492. [[CrossRef](#)] [[PubMed](#)]
19. Yang, Y.; Wang, W.; Boulesbaa, A.; Kravchenko, I.I.; Briggs, D.P.; Puretzky, A.; Geohegan, D.; Valentine, J. Nonlinear Fano-resonant dielectric metasurfaces. *Nano Lett.* **2015**, *15*, 7388–7393. [[CrossRef](#)] [[PubMed](#)]
20. Shorokhov, A.S.; Melik-Gaykazyan, E.V.; Smirnova, D.A.; Hopkins, B.; Chong, K.E.; Choi, D.Y.; Shcherbakov, M.R.; Miroshnichenko, A.E.; Neshev, D.N.; Fedyanin, A.A.; et al. Multifold Enhancement of Third-Harmonic Generation in Dielectric Nanoparticles Driven by Magnetic Fano Resonances. *Nano Lett.* **2016**, *16*, 4857–4861. [[CrossRef](#)] [[PubMed](#)]
21. Chen, S.; Rahmani, M.; Li, K.F.; Miroshnichenko, A.; Zentgraf, T.; Li, G.; Neshev, D.; Zhang, S. Third Harmonic Generation Enhanced by Multipolar Interference in Complementary Silicon Metasurfaces. *ACS Photonics* **2018**, *5*, 1671–1675. [[CrossRef](#)]
22. Grinblat, G.; Li, Y.; Nielsen, M.P.; Oulton, R.F.; Maier, S.A. Enhanced third harmonic generation in single germanium nanodiscs excited at the anapole mode. *Nano Lett.* **2016**, *16*, 4635–4640. [[CrossRef](#)] [[PubMed](#)]

23. Shibanuma, T.; Grinblat, G.; Albella, P.; Maier, S.A. Efficient Third Harmonic Generation from Metal—Dielectric Hybrid Nanoantennas. *Nano Lett.* **2017**, *17*, 2647–2651. [[CrossRef](#)] [[PubMed](#)]
24. Vabishchevich, P.P.; Liu, S.; Sinclair, M.B.; Keeler, G.A.; Peake, G.M.; Brener, I. Enhanced second-harmonic generation using broken symmetry III–V semiconductor fano metasurfaces. *ACS Photonics* **2018**, *5*, 1685–1690. [[CrossRef](#)]
25. Xu, L.; Rahmani, M.; Zangeneh Kamali, K.; Lamprianidis, A.; Ghirardini, L.; Sautter, J.; Camacho-Morales, R.; Chen, H.; Parry, M.; Staude, I.; et al. Boosting third-harmonic generation by a mirror-enhanced anapole resonator. *Light Sci. Appl.* **2018**, *7*, 44. [[CrossRef](#)]
26. Boyd, R.W. *Nonlinear Optics*; Academic Press: New York, NY, USA, 2008.
27. Shcherbakov, M.R.; Liu, S.; Zubyuk, V.V.; Vaskin, A.; Vabishchevich, P.P.; Keeler, G.; Pertsch, T.; Dolgova, T.V.; Staude, I.; Brener, I.; et al. Ultrafast all-optical tuning of direct-gap semiconductor metasurfaces. *Nat. Commun.* **2017**, *8*, 17. [[CrossRef](#)] [[PubMed](#)]
28. Carletti, L.; Locatelli, A.; Stepanenko, O.; Leo, G.; De Angelis, C. Enhanced second-harmonic generation from magnetic resonance in AlGaAs nanoantennas. *Opt. Express* **2015**, *23*, 26544–26550. [[CrossRef](#)] [[PubMed](#)]
29. Gili, V.; Carletti, L.; Locatelli, A.; Rocco, D.; Finazzi, M.; Ghirardini, L.; Favero, I.; Gomez, C.; Lemaître, A.; Celebrano, M.; et al. Monolithic AlGaAs second-harmonic nanoantennas. *Opt. Express* **2016**, *24*, 15965–15971. [[CrossRef](#)] [[PubMed](#)]
30. Liu, S.; Sinclair, M.B.; Saravi, S.; Keeler, G.A.; Yang, Y.; Reno, J.; Peake, G.M.; Setzpfandt, F.; Staude, I.; Pertsch, T.; et al. Resonantly enhanced second-harmonic generation using III–V semiconductor all-dielectric metasurfaces. *Nano Lett.* **2016**, *16*, 5426–5432. [[CrossRef](#)] [[PubMed](#)]
31. Camacho-Morales, R.; Rahmani, M.; Kruk, S.; Wang, L.; Xu, L.; Smirnova, D.A.; Solntsev, A.S.; Miroshnichenko, A.; Tan, H.H.; Karouta, F.; et al. Nonlinear generation of vector beams from AlGaAs nanoantennas. *Nano Lett.* **2016**, *16*, 7191–7197. [[CrossRef](#)] [[PubMed](#)]
32. Carletti, L.; Locatelli, A.; Neshev, D.; De Angelis, C. Shaping the Radiation Pattern of Second-Harmonic Generation from AlGaAs Dielectric Nanoantennas. *ACS Photonics* **2016**, *3*, 1500–1507. [[CrossRef](#)]
33. Ghirardini, L.; Carletti, L.; Gili, V.; Pellegrini, G.; Duò, L.; Finazzi, M.; Rocco, D.; Locatelli, A.; De Angelis, C.; Favero, I.; et al. Polarization properties of second-harmonic generation in AlGaAs optical nanoantennas. *Opt. Lett.* **2017**, *42*, 559–562. [[CrossRef](#)] [[PubMed](#)]
34. Timofeeva, M.; Lang, L.; Timpu, F.; Renaut, C.; Bouravleuv, A.; Shtrom, I.V.; Cirlin, G.; Grange, R. Anapoles in Free-Standing III-V Nanodiscs Enhancing Second-Harmonic Generation. *Nano Lett.* **2018**, *18*, 3695–3702. [[CrossRef](#)] [[PubMed](#)]
35. Shoji, I.; Kondo, T.; Kitamoto, A.; Shirane, M.; Ito, R. Absolute scale of second-order nonlinear-optical coefficients. *JOSA B* **1997**, *14*, 2268–2294. [[CrossRef](#)]
36. Ohashi, M.; Kondo, T.; Ito, R.; Fukatsu, S.; Shiraki, Y.; Kumata, K.; Kano, S. Determination of quadratic nonlinear optical coefficient of $\text{Al}_x\text{Ga}_{1-x}\text{As}$ system by the method of reflected second harmonics. *J. Appl. Phys.* **1993**, *74*, 596–601. [[CrossRef](#)]
37. Melik-Gaykazyan, E.V.; Kruk, S.S.; Camacho-Morales, R.; Xu, L.; Rahmani, M.; Zangeneh Kamali, K.; Lamprianidis, A.; Miroshnichenko, A.E.; Fedyanin, A.A.; Neshev, D.N.; et al. Selective third-harmonic generation by structured light in Mie-resonant nanoparticles. *ACS Photonics* **2017**, *5*, 728–733. [[CrossRef](#)]
38. Carletti, L.; Koshelev, K.; De Angelis, C.; Kivshar, Y. Giant nonlinear response at the nanoscale driven by bound states in the continuum. *arXiv* **2018**, arXiv:1804.02947.
39. Camacho-Morales, R.; Bautista, G.; Zang, X.; Xu, L.; Turquet, L.; Miroshnichenko, A.; Lamprianidis, A.; Rahmani, M.; Neshev, D.N.; Kauranen, M. Resonant harmonic generation in AlGaAs nanoantennas using cylindrical vector beams. In Proceedings of the CLEO: QELS_Fundamental Science, Optical Society of America, San Jose, CA, USA, 13–18 May 2018; p. FF1E–6.
40. Yang, Y.; Miroshnichenko, A.E.; Kostinski, S.V.; Odit, M.; Kapitanova, P.; Qiu, M.; Kivshar, Y.S. Multimode directionality in all-dielectric metasurfaces. *Phys. Rev. B* **2017**, *95*, 165426. [[CrossRef](#)]

